Finite element modelling of the inertia friction welding of a CrMoV alloy steel including the effects of solid-state phase transformations

C. Bennett

Department of Mechanical,

Materials and Manufacturing Engineering,

University of Nottingham,

Nottingham NG7 2RD, UK

Abstract

Finite element (FE) process modelling of the inertia friction welding (IFW) between two tubular CrMoV components has been carried out using the DEFORM-2D (v10.2) software. This model has been validated against experimental test welds of the material; this included process data such as upset and rotational velocity as well as thermal data collected during the process using embedded thermocouples. The as-welded residual stress from the FE model has been compared to experimental measurements taken on the welded component using the hole drilling technique. The effects of the solid-state phase transformations which occur in the steel are considered and the trends in the

residual stress measurements were well replicated when compared to the experimental data.

Keywords: inertia friction welding; finite element; phase transformations; residual stress

1 Introduction

Inertia friction welding (IFW) is a quick and repeatable solid state joining technique which can be used to join a wide range of materials in both similar or dissimilar joints [1] avoiding bulk melting of material. Due to the high energy input rates in the process, IFW produces welds with steep thermal gradients around the interface which results in a narrow heat affected zone (HAZ). The HAZ is generally defined as the region the region of material which has undergone significant structural changes due to the welding process [2] and in IFW can encompass the bond line, the thermo-mechanically affected zone (TMAZ), where large deformations occur, and the region purely thermally affected next to the base material. There are three controllable parameters in inertia friction welding; these are rotational velocity, flywheel inertia and the axial pressure applied to the weld. The weld duration, energy input rate and deformation levels during the welding process can be controlled by varying the parameters [3]. Due to the high temperatures, deformations and subsequent thermal contraction of the weld during cooling, residual stress is induced in the material in and around the weld region.

The modelling of manufacturing processes can allow a greater degree of

understanding and insight to be gained than solely through the inspection of completed parts due to the information that can be extracted from the model such as full field residual stress, strain and temperature results and the variation in these fields with changing parameters. All of this can be achieved using a process model without the expense and lead time associated with producing actual components and performing post manufacturing analysis.

Process modelling is particularly useful for IFW as it is a rapid, complex, coupled thermo-mechanical process that is highly dependent on the input parameters. The welds of interest in this study were like-to-like welds of a high strength chromium, molybdenum, vanadium (CrMoV) alloy steel (0.4C, 3.35Cr, 0.4Ni, 1.15Mo, 0.26Mn, 0.15Si, 0.17V).

The modelling of IFW has been addressed by a number of authors using a variety of different approaches; initial models created in the 1970s were purely thermal models using the finite difference method [4, 5]. A heat flux which was a function of rotating speed and distance from the centre was applied at the interface and their models highlighted the presence of high heating rates and steep thermal gradients near the interface.

Analytical modelling of the thermal effects of the process was carried out by Davé et al. [6] in 2001 to provide guidance in the selection of weld parameters for the welding of dissimilar materials (Nb to 316SS in this case). The energy used to expel the flash was estimated in this case and then the resulting thermal profile was calculated. The thermal input was derived directly from the angular speed curve obtained from an experimental weld. Two models were proposed and the results were compared to the thermal data obtained from welds. The difference between the two models and measured

experimental temperature data was a maximum of 100 and 350°C for the two techniques.

Later developed fully-coupled thermo-mechanical models of the IFW process mainly use two approaches to the treatment of the interface, the first of these being to use existing experimental data which is then converted to a heat flux at the interface [7, 8], this allows existing welds for which data is available to be recreated in a model to obtain an accurate representation of deformations and thermal fields during the process. The second approach is the inclusion of a friction law [9, 10, 11] based on the current conditions at the interface, which removes the requirement for existing weld data and leads to the development of a predictive capability.

A fully coupled thermo-mechanical finite element model of the IFW process was developed by Moal and Massoni [9]. The code (INWELD) included adaptive re-meshing and although axi-symmetric included the circumferential velocity component which lead to a 2.5D model capable of predicting the slowdown of the flywheel. This work considered a nickel-based alloy, NK17CDAT and the results of the model were compared with actual industrial welds where the rotational speed values compared well but the axial shortening of the welds were overestimated by 20%. This work did not consider the development of residual stresses during the post-weld cooling phase. The DEFORM-2D code was extended in 2001 by Lee et al. [12] in a similar way to include torsional effects and a special axi-symmetric element (again 2.5D) was developed with three velocity components but no velocity gradients in the circumferential direction.

D'Alvise et al. [10] extended the work of Moal and Massoni [9] by includ-

ing a new mathematical formulation and subsequently an extension to account for dissimilar material weld combinations by developing a specific coupled thermo-mechanical finite element module implemented in the FORGE2 commercial code in 2002 to perform analysis of the IFW process. Mechanical equations taking into account the inertia, forces and friction were included in the model. A friction law based on pressure, rotational speed and temperature was proposed to represent the interface contact during the weld period. Similar and dissimilar nickel-based alloy materials and geometry welds were investigated and weld time, upset and thermal results from the model were compared with experimental measurements taken during the welding process. In all cases the model over predicted the values when compared to those from the welds. However the variation in the results across seven different welds, with different parameters, compared well.

Modelling of the IFW of the nickel-based superalloy RR1000 was carried out using a fully coupled thermo-mechanical model developed in DEFORM-2D by Wang et al. [7] and Grant et al. [8]. These works considered the build-up of residual stresses in the components by modelling the post-weld cooling phase using an elastic-plastic material model. The approach used in both of these pieces of work for the welding modelling was to determine the energy input rate from experimental data and covert this to a thermal boundary at the interface. The residual stress in the model of Wang et al. [7] were over predicted by around 35% in the as-welded and cooled state; however no machining was performed on the model before the comparison was made with experimental results, where some machining of the weld had occurred. An improved material database was used by Grant et al. [8] and

an improved match to the experimental residual stress results was achieved. Microstructural analyses were carried out on welds an a good match in peak temperatures inferred from the presence of gamma prime phases (approximately 20°C difference) was seen. Comparison of the γ' precipitation variation across the weld line and the microstructure produced by fast heating and cooling experiments following predicted temperature profiles also showed good agreement.

An analysis of the microstructure evolution of the FGH96 superalloy, with a particular focus on dynamic recrystallisation (DRX) and grain size prediction was carried out by Nie et al. [13] using the MSc.Marc software. Microstructure predictions were made using a basic DRX model fitted to data generated using a Gleeble 1500 thermo-mechanical simulator and were qualitatively compared with the results of experimental welds and showed reasonable agreement.

The importance of solid-state phase transformations on the residual stresses generated in inertia friction welds between a high strength steel (AerMet 100) and a nickel-based superalloy (Inconel 718) has been discussed previously [11], however no comparisons were made with any experimental residual stress values.

The current work uses the additional capability added to the DEFORM-2D software by Lee et al. [12] to perform fully coupled thermo-mechanical finite element analyses of the IFW process for CrMoV steel including both workpieces. As well as the welding phase, the post-weld cooling phase is also modelled in order to evaluate the residual stresses generated during the welding of the component by use of the thermal profile which exists at the

end of the welding process. The effect of solid-state phase transformations is included in the model as these have been shown to have an important effect on the residual stresses generated during cooling of steel welds and the residual stress profiles from this model are compared with experimental hole drilling investigations on actual welds of the material. Weld data is used to create models with improved accuracy in terms of temperatures, phase volume distribution and deformations when compared to existing modelling techniques which usually result in a good match of a limited number of outputs and while the implementation is not a fully predictive approach, this strategy allows a wide variety of information to be gained from the models, including variations of temperature, residual stress and phase information throughout the entire welded components. Accurate predictions of these quantities is important in industrial applications due to their implications on the performance and life of components in service.

2 Experimental Procedures

2.1 Test welds

Two test welds between two identical CrMoV steel components were carried out in order to provide information for and to validate the process model being developed. These welds were instrumented with thermocouples during welding and were also subject to residual stress characterization using the hole drilling technique [14] in the as-welded state to compare directly with the model outputs.

2.1.1 Geometry

The parts welded for this study were cylindrical components with weld interface geometries with an outer diameter (OD) of 50 mm and a wall thickness of 16 mm. An overview of the weld specimen geometry is given in Figure 1

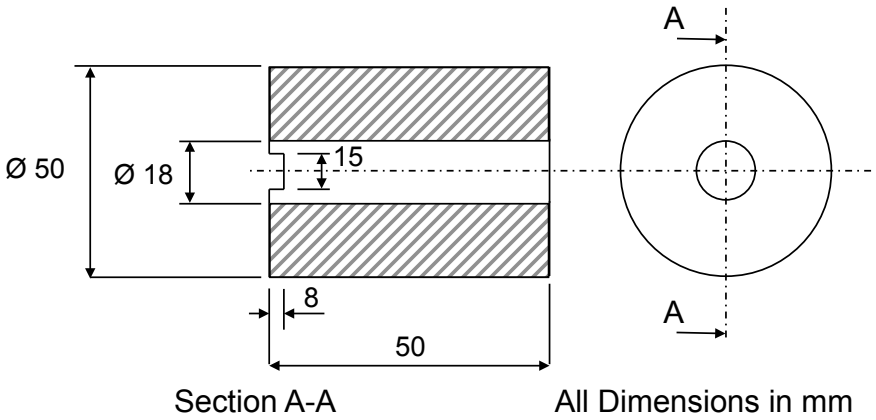

Figure 1: Weld Specimen Geometry

2.1.2 Weld parameters

Weld parameters for the welds considered in this work are presented in Table 1.

Table 1: Weld Parameters

Parameter	Weld 1	Weld 2
Initial Speed, ω [rad s^{-1}]	122.6	122.6
Flywheel Inertia, I [kg m^2]	30.97	30.97
Weld Pressure, P_0 [MPa]	228	448

The total energy, stored in the flywheel, available for welding (E) can be calculated using:

$$E = \frac{1}{2} I \omega^2 \tag{1}$$

where I is the flywheel inertia and ω is the initial rotational velocity of the flywheel.

The nominal weld pressure, P_0, is determined using the initial contact area, A_0, from the pre-weld workpiece geometry and the axial force, F, applied by the welding machine and can be calculated by:

$$P_0 = \frac{F}{A_0} \tag{2}$$

From Table 1 it can be seen that the total energy for both of the welds is identical while the weld pressure for Weld 2 is approximately double that of Weld 1.

2.1.3 Temperature measurements

Thermocouples (type K) with a diameter of 0.5mm were embedded in the non-rotating side of Weld 1 and used to measure the mid-wall temperature during the weld at locations 3, 5 and 15mm from the initial weld interface.

3 Model Details

Modelling of the inertia friction welding process has been carried out using the DEFORM-2D (v10.2) commercial, forming, finite element package which was extended in 2001 by Lee et al. [12] to include torsional effects by introducing a special 2.5D element which includes three velocity components (radial (r), axial (z) and circumferential (θ) but no velocity gradient in the circumferential direction.

The weld process has been modelled in four phases which involve different modelling strategies, the first two phases make up the two parts of the weld process as shown in Figure 2. These are (i) the heating, or conditioning phase and (ii) the deformation, or upsetting phase. The first phase (i) is modelled to establish the temperature field within the components while the components deformations are prescribed in the second phase (ii).

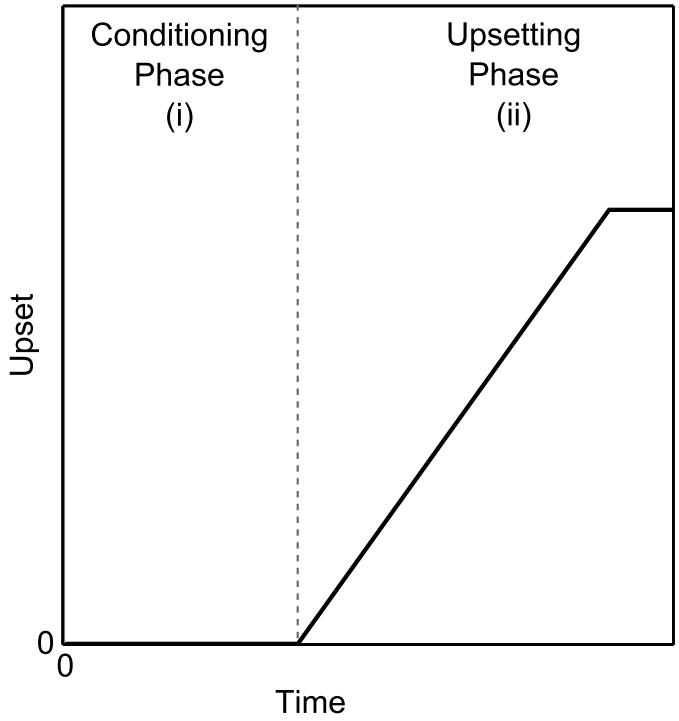

Figure 2: Weld Phases

Additional phases modelled are the cooling phase (iii) which begins when all of the energy is dissipated from the flywheel and the machining phase (iv) which is carried out before residual stress data is extracted from the models. Both components are modelled (fixture and spindle workpieces) as shown in the overview given in Figure 3.

The transition between phases (i) and (ii) is governed by the onset of deformation from the experimental data. The transition from phase (ii) to (iii) occurs when all energy has been dissipated from the flywheel. For the initial part of phase (iii) (45 s) the axial load is maintained and is then removed for the remainder of the cooling period (1500 s in total). In phase (iv) a boolean operation is performed to remove material to simulate the machining process and the results from the pre-machined model are then interpolated onto this new geometry and 10 stress re-distribution time-steps are run to ensure that an equilibrium condition is reached.

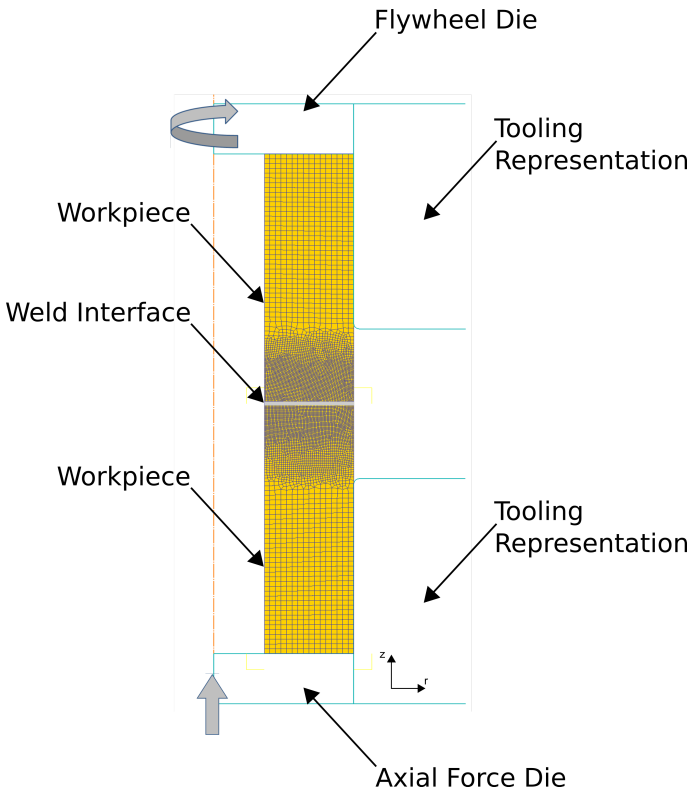

Figure 3: General IFW Model Overview

3.1 Boundary conditions

At the contacting surface between the components, the friction coefficient is defined as a function of time and is calculated from the experimental flywheel rundown data using the following relationship [12]:

$$\mu_n = \eta \frac{E_{n+1} - E_n}{-\omega_n \Delta t p(\frac{2\pi}{3}[r_o^3 - r_i^3])} \tag{3}$$

During the calculation of these values a constant pressure, p, and contact area are assumed between the two components. η is the efficiency factor and the subscripts n and $n+1$ denote the current and next time increment respectively. The calculated friction coefficient data (assuming η=1.0) for the two welds are presented in Figure 4. It can be seen that the lower value of pressure for Weld 1 results in a lower energy input rate meaning that the time required to dissipate all of the energy from the system is longer, hence the longer weld time. It is worth noting however that the values of friction coefficient for the two welds are similar suggesting similar interface conditions are present during the welding.

The rotational velocity of the flywheel and therefore the associated workpiece is prescribed throughout the process in accordance with the experimental weld speed run down curve.

During the conditioning phase (i), an axial force in accordance with the weld parameters is applied to the primary die to ensure that the correct heating is calculated during this phase.

During the upsetting phase (ii), the axial displacement rate, calculated from the weld data, is applied to the primary die to ensure that the correct

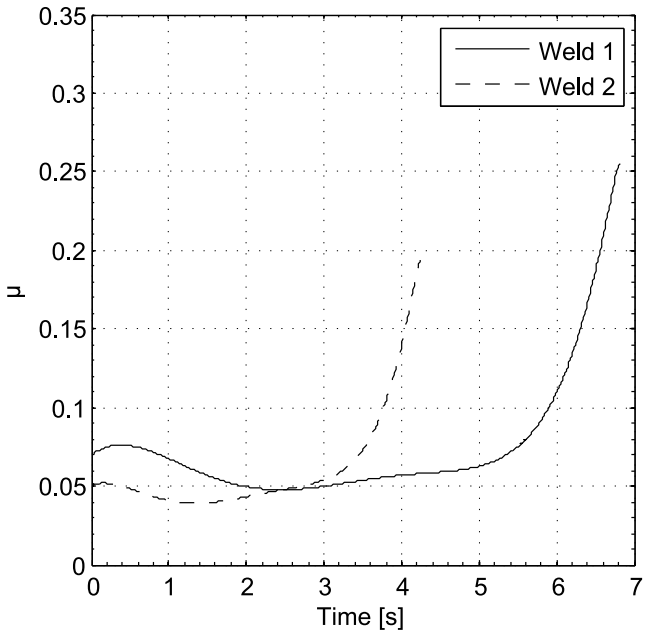

Figure 4: Calculated Friction Coefficient

level and rate of deformation is applied to the workpieces during the weld.

Throughout the analyses, a sticking condition is applied between the workpieces and the dies to ensure that rotation and axial force/movement is applied from the dies to the workpieces.

3.2 Material properties

Due to the wide range of temperatures, strain rates and large strains experienced by the material during inertia friction welding, an extensive material database is required to represent the material in the finite element model. During the weld process (phases (i) and (ii)), the workpieces are modelled as rigid-plastic bodies as the large deformations which occur in the interface region ensure that the total strain is well approximated by the plastic strain. For the modelling of the cooling (phase iii) and machining (phase iv)

the material model is switched to elastic-plastic to allow the build up and redistribution of residual stresses.

3.2.1 Mechanical properties

Axisymmetric compression testing is commonly used to determine the flow stress of materials for materials forming and forging modelling, this testing was carried out on the CrMoV steel and this experimental data was then processed and extrapolated to cover the range of temperatures, strains and strain rates which it was expected to be experienced during the process, this extrapolation aspect also ensures stability of the solution procedure when running the FE model. The yield stress and Young's Modulus variation with temperature from the database is presented in Figure 5 to illustrate the variation in material properties across the temperature range.

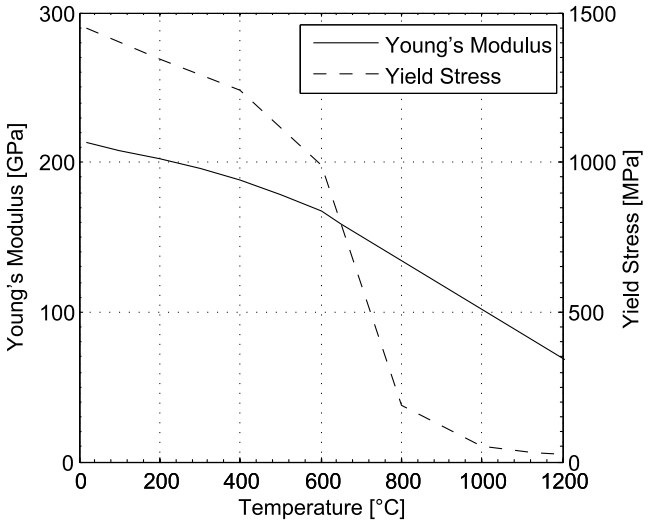

Figure 5: CrMoV Young's Modulus and Yield Stress Variation with Temperature

3.2.2 Thermal properties

Temperature dependent heat capacity and thermal conductivity for the CrMoV steel used in the modelling are presented in Figure 6.

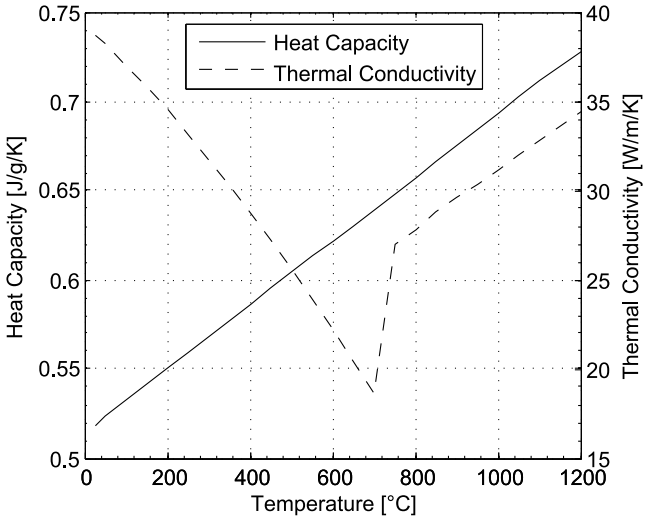

Figure 6: CrMoV Thermal Properties

3.2.3 Solid-state phase transformations

The CrMoV steel undergoes solid state phase transformations during the heating and cooling cycle which it experiences during the welding process. On heating the material transforms from the base material of tempered martensite to austenite over the approximate temperature range 830-900°C (at representative heating rates), this material then transforms back to (quenched) martensite on cooling, beginning at around 300°C. These transformations are shown schematically in dilatometry data in Figure 7, where Ac1 and Ac3 are the start and finish temperatures of the transformation to austenite on heating and M_s and M_f are the marstensite start and finish temperatures

on cooling. These transformations have been included in the finite element model of the IFW process using the DEFORM-HT add on to the base software to create a dual phase material (austenite & martensite) that will be used to investigate the transformation between the phases during the weld.

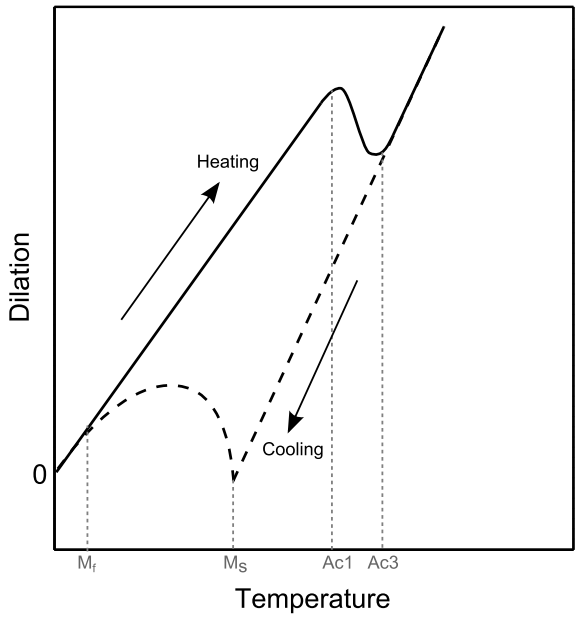

Figure 7: Relevant phase transformations in the CrMoV steel as depicted in schematic dilatometry data

The kinetics of the transformation to austenite on heating is included in DEFORM using a diffusion type function of the form [15]:

$$\xi_J = 1 - exp\left[A\left(\frac{T - T_s}{T_e - T_s}\right)^D\right] \tag{4}$$

The coefficients of the function, A and D, along with T_s and T_e, the start and end temperatures respectively, have been determined from experimental dilatometry data. The data was converted into phase volume fraction data over the transformation range, using the lever rule, this assumes that the

volume fraction of transformed material is proportional to the fraction of the total volume change that has occurred at any instant.

The transformation to martensite on cooling is represented using the martensitic transformation function [15]:

$$\xi_M = 1 - exp[\psi_1 T + \psi_2(C - C_0) + \psi_{31}\sigma_m + \psi_{32}\bar{\sigma} + \psi_4] \tag{5}$$

for the purpose of this work it is assumed that there is no dependency on the carbon content, due to the short time at high temperatures during the welding, or stress on the martensite transformation and therefore ψ_2, ψ_{31} and ψ_{32} take a value of 0 and Equation 5 reduces to

$$\xi_M = 1 - exp[\psi_1 T + \psi_4] \tag{6}$$

The coefficients that define the solid-state phase transformations in the CrMoV steel for Equations 4 and 6 are presented in Table 2.

Table 2: Coefficients to define Solid-State Phase Transformations in CrMoV Steel

Parameter	Value
A	-4.94
D	2.09
T_s	834
T_e	902
ψ_1	0.014
ψ_4	-4

3.3 Mesh Design

A fine mesh of 0.25 mm is used in the region of the interface throughout all of the analyses in order to capture the large deformation that occur in this region, while a much larger mesh is used in the far field region (1mm) in order to reduce the total number of elements in the analyses and reduce the overall computation time. The initial mesh can be viewed in Figure 3. Re-meshing is performed at total upset increments of 0.5 mm to ensure that the elements retain their shape. This mesh design is consistent with previous work of this kind [11].

3.4 Efficiency

The efficiency factor, η, accounts for the mechanical losses present in the welding machine to ensure that the correct portion of the total energy is input into the weld. The efficiency of the welding process was determined by comparing the temperature values from the phase (i) model with the temperature data collected from the embedded thermocouples of Weld 1.

The comparison of the temperatures extracted from three different phase (i) models of Weld 1 using different values of efficiency are compared with the experimental temperature data after 1.5s of weld time in Figure 8, by examining these results, an efficiency of 70% was found to provide adequate thermal results during the conditioning phase based primarily on the experimental datapoint closest to the interface as this location will be less affected by errors due to thermal conduction within the component. This value of efficiency has been used across all of the models presented here.

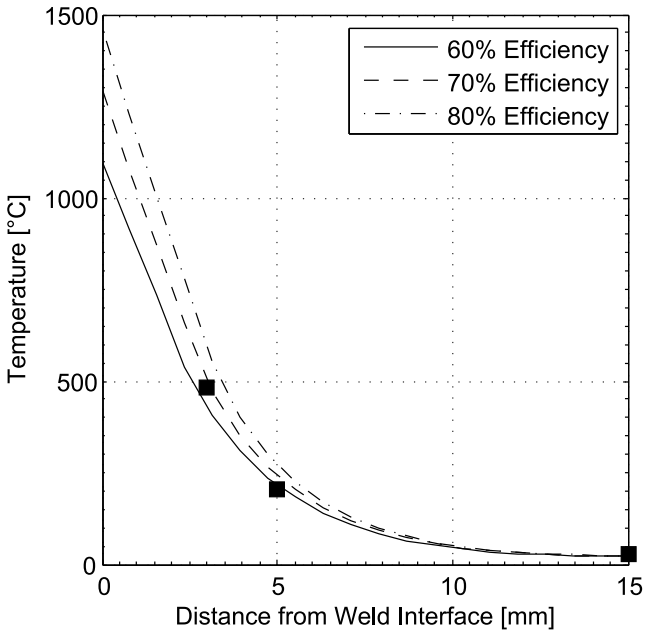

Figure 8: Comparison of Temperature Profiles in Weld 1 model at a weld time of 1.5s (end of conditioning)

4 Results and Discussion

4.1 Temperature

A comparison between the temperature profile and heating rate extracted from the models at the end of conditioning is presented in Figure 9. It can be seen that the higher axial load applied to Weld 2 results in a higher peak temperature of around 100°C at the interface along with a far higher heating rate close to the interface, while further away from the weld interface (>5mm), as a result of the longer conditioning period of Weld 1 (1.5s vs the 0.75s of Weld 2) due to the reduced energy input rate caused by the lower pressure meaning the material close to the interface requires a longer time to reach the forging temperatures required for the deformation to begin (end of

conditioning), the conduction effects dominate and the heating rate is higher in this region.

4.2 Axial Load

The axial load from the deformation phase of the two weld models are presented in Figure 10 and are compared with the nominal experimental value from the weld parameters given in Table 1. Following an initial over-prediction of load from the model in both cases the value settles to match the nominal experimental load to within 10% for both welds. The load reduces at the end of the process where no load is required as the deformation rate falls to zero when the rotation has stopped and the weld begins to cool. The mean loads from the models vary from the nominal experimental load by +6% and -6% for Weld 1 and 2 respectively. The purpose of this model is to ensure that the deformation levels of the two models are equivalent to the experimental data to ensure that the effects of the correct strains and component shape are reflected in the residual stress prediction. It is however encouraging to note that the forging loads required to achieve those deformation levels match well with the applied experimental values.

4.3 Phase Volume Fraction

Figure 11 presents the austenite volume fraction in the weld region at the end of the weld (phase (ii)) before cooling and is indicative of the volume of material which will transform to martenstite upon cooling (phase (iii)). It can be seen that the higher pressure weld (Weld 2) results in a narrower region of

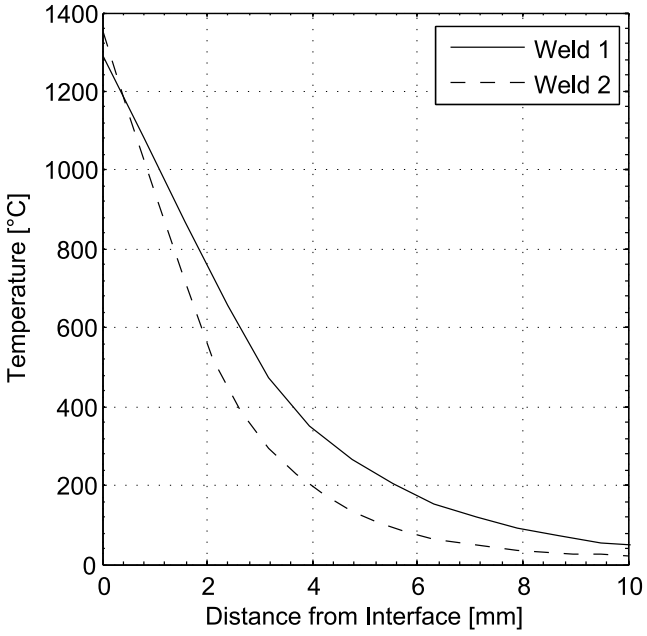

(a)

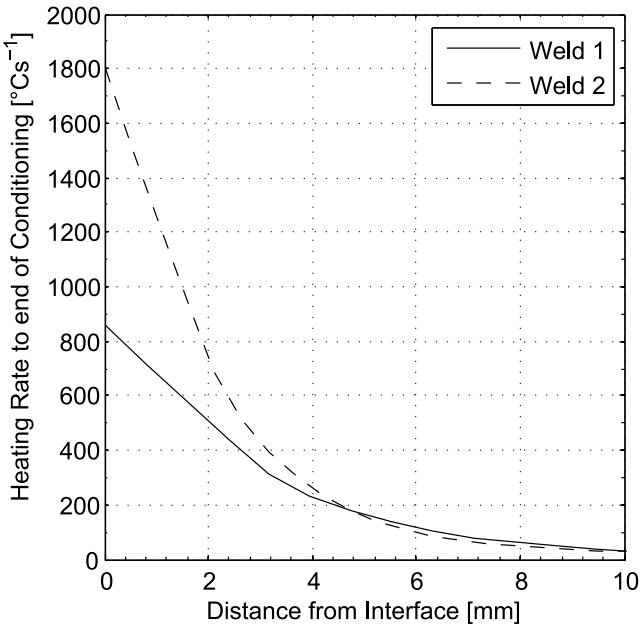

(b)

Figure 9: Comparison of (a) Temperature Profile and (b) Heating Rate at the end of Conditioning for both welds

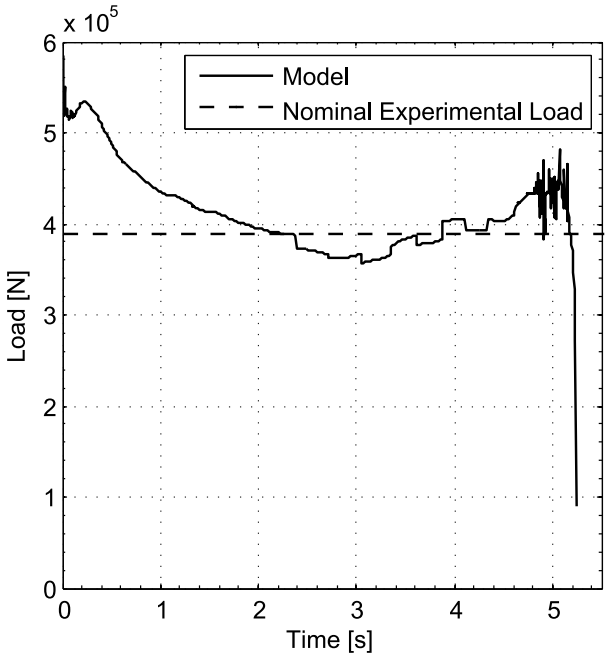

(a)

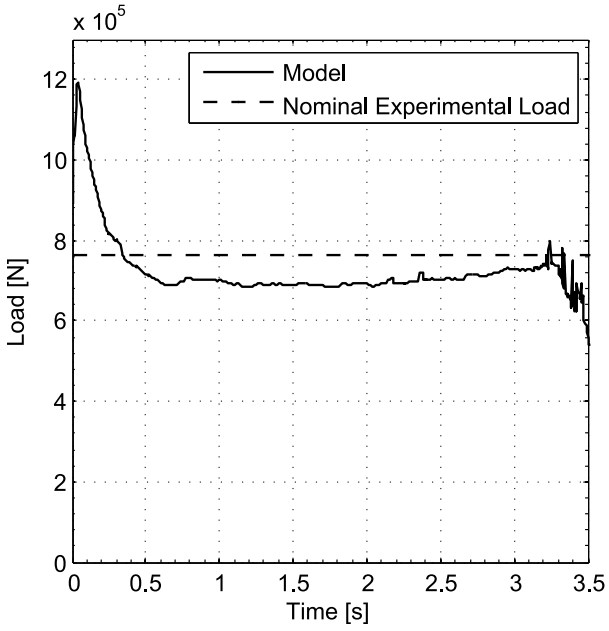

(b)

Figure 10: Comparison of Model and Experimental Nominal axial load during deformation phase of (a) Weld 1 and (b) Weld 2

austenite material, approximately 5mm across compared to around 8mm in Weld 1. This is also highlighted in Figure 12 which shows the volume fraction variation with distance from the weld line near the OD of the components for both welds, this location is consistent with where the hole drilling data has been taken for the residual stress measurements. This data is compared with the micro structural cross section for Weld 1 in Figure 13 where it can be seen that the width of the region of material which transforms to austenite on heating can clearly be seen to match closely to the corresponding width of affected material from the weld cross-section.

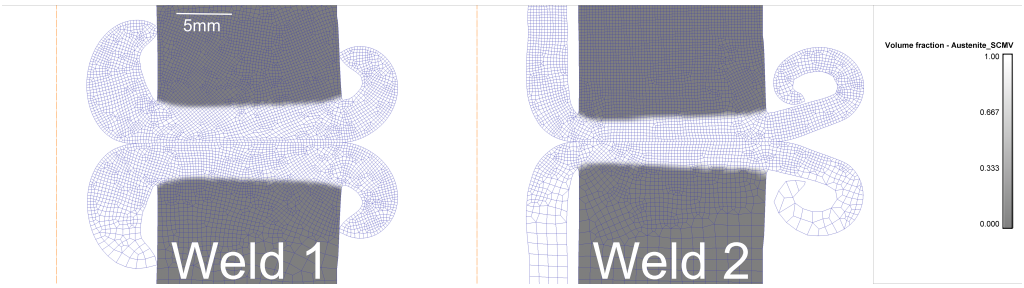

Figure 11: Comparison of austenite region in both welds (end of welding)

4.4 Residual Stress

Hoop residual stress profiles have been extracted from the models in the as-welded, cooled and machined state (after phase (iv)) to compare with hole drilling data obtained from the experimental welds and are presented in Figure 14.

This shows a 25% under-prediction for Weld 1 in the maximum value of hoop residual stress and a 16% over-prediction for Weld 2. The axial location of the peak stress value is well predicted for Weld 1 and the peak

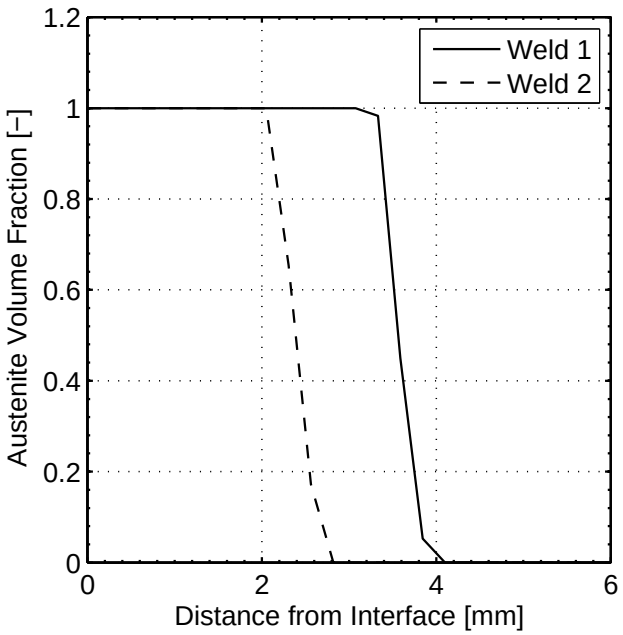

Figure 12: Variation in austenite volume fraction near the OD with distance from weld interface in both welds (end of welding)

has shifted towards the weld line in Weld 2 in accordance with the narrowing of the austenite region presented in Figures 11 and 12, however it has not moved close enough to the weld line when compared with the experimental values. In the case of Weld 2, no temperature data were available to calibrate the model and the same value of efficiency was assumed as with Weld 1. Considering the data presented in Figure 12 in conjunction with the residual stress data confirms that the reduction in stress around the weld line is consistent with the region which has transformed to austenite on heating and therefore will have transformed to martensite on cooling and been subjected to the corresponding volume change, causing a stress relief effect in this region, this also shows that the peak stress is located at the edge of the HAZ and therefore suggests an over-prediction of the width of the HAZ of less

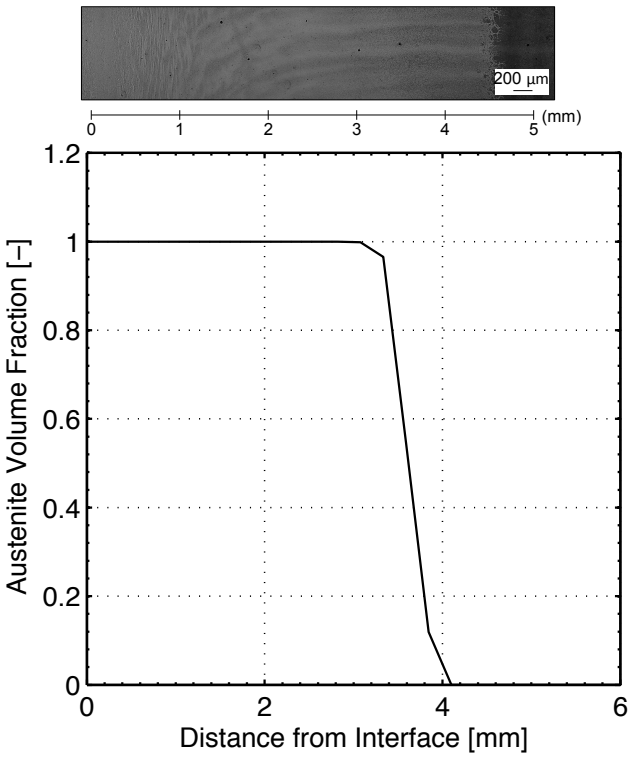

Figure 13: Comparison of weld cross section showing HAZ with austenite volume fraction for Weld 1

than 1mm for Weld 2.

5 Conclusions

A four stage modelling process has been presented which can be used to accurately represent the thermal and mechanical aspects of the inertia friction welding process through the use of load and displacement controlled phases. Thermal results from the first phase of the model for two different weld parameters have shown a significant difference in heating rate between the two welds and approximately 100°C difference in interface temperature. The thermal profile and deformed weld shape at the end of the welding process has been used to predict the residual stresses in the remaining two phases of the model which simulate the post-weld cooling and machining of the finished component. Results from the phase volume fields show that the higher weld pressure of Weld 2 results in a narrower HAZ region which is confirmed by the predictions and measurement of the residual stress where the comparison shows that the peak values are well predicted by the model and in the case of Weld 1, where thermal data is available to allow calibration of the model, the HAZ width is well predicted. The HAZ width was reduced in the model when a higher pressure was used for the welding, which is consistent with the shifting of the peak in the experimental hole drilling results, however the model overestimated the HAZ width in this case by less than 1mm.

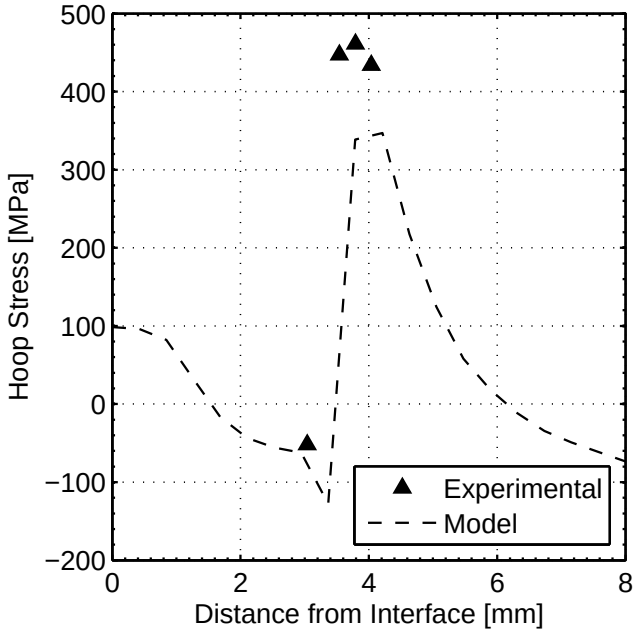

(a)

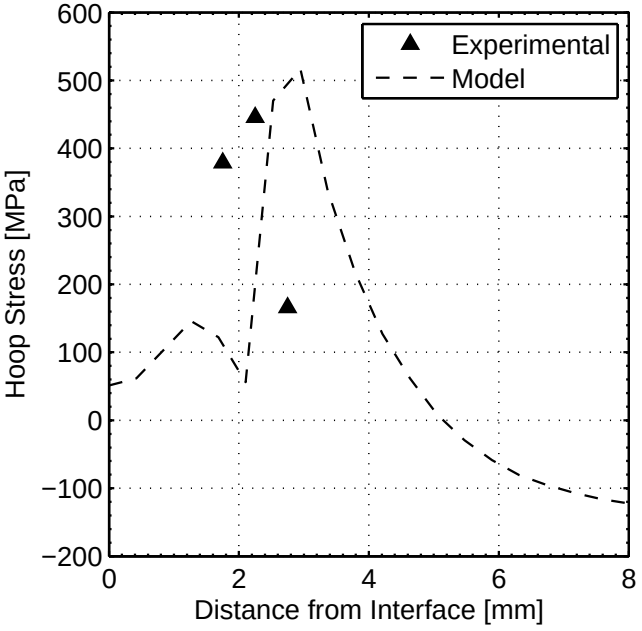

(b)

Figure 14: Comparison of hoop residual stress profiles with experimental hole drilling data for Weld 1 (a) and Weld 2 (b)

Acknowledgements

The authors wish to thank Rolls-Royce plc, Aerospace Group, for their financial support of the research, which was carried out at the University Technology Centre in Gas Turbine Transmission Systems at the University of Nottingham. The views expressed in this paper are those of the authors and not necessarily those of Rolls-Royce plc, Aerospace Group.

References

[1] C. Weismann, Resistance and solid state welding and other joining processes, Vol. 3 of Welding Handbook, American Welding Society, 1976.

[2] T. Debroy, J. Szekely, T. Eagar, Temperature profiles, the size of the heat-affected zone and dilution in electroslag welding, Materials Science and Engineering 56 (2) (1982) 181–193,

[3] M. Preuss, P. Threadgill, Solids State Wedling of Aerospace Materials, Encyclopedia of Aerospace Engineering, John Wiley & Sons Ltd, 2010.

[4] K. K. Wang, P. Nagappan, Transient temperature distribution in inertia friction welding of steels, Welding Journal 49(9) (1970) 419s–426s.

[5] K. K. Wang, W. Lin, Flywheel friction welding research, Welding Journal 53 (1974) 233s–241s.

[6] V. Dave, M. Cola, G. Hussen, Heat generation in the inertia welding of dissimilar tubes, Welding Journal (Miami, Fla) 80 (10) (2001) 246s – 252s.

[7] L. Wang, M. Preuss, P. Withers, G. Baxter, P. Wilson, Energy-input-based finite-element process modeling of inertia welding, Metallurgical and Materials Transactions B: Process Metallurgy and Materials Processing Science 36 (4) (2005) 513 – 523.

[8] B. Grant, M. Preuss, P. Withers, G. Baxter, M. Rowlson, Finite element process modelling of inertia friction welding advanced nickel-based superalloy, Materials Science and Engineering A 513-514 (C) (2009) 366 – 375.
URL http://dx.doi.org/10.1016/j.msea.2009.02.005

[9] A. Moal, E. Massoni, Finite element simulation of the inertia welding of two similar parts, Engineering Computations 12 (6) (1995) 497 – 512.

[10] L. D'Alvise, E. Massoni, S. Walloe, Finite element modelling of the inertia friction welding process between dissimilar materials, Journal of Materials Processing Technology 125-126 (2002) 387 – 391.
URL http://dx.doi.org/10.1016/S0924-0136(02)00349-7

[11] C. J. Bennett, T. H. Hyde, E. J. Williams, Modelling and simulation of the inertia friction welding of shafts, Proceedings of the Institution of Mechanical Engineers, Part L: Journal of Materials Design and Applications 221 (4) (2007) 275–284. arXiv:http://pil.sagepub.com/content/221/4/275.full.pdf+html, doi:10.1243/14644207JMDA154.
URL http://pil.sagepub.com/content/221/4/275.abstract

[12] K. Lee, K. Samant, W. T. Wu, S. Srivatsa, Finite finite element modelling of inertia welding processes, in: NUMIFORM, 2001.

[13] L. Nie, L. Zhang, Z. Zhu, W. Xu, Microstructure evolution modeling of {FGH96} superalloy during inertia friction welding process, Finite Elements in Analysis and Design 80 (0) (2014) 63 – 68. doi:http://dx.doi.org/10.1016/j.finel.2013.10.007.
URL http://www.sciencedirect.com/science/article/pii/S0168874X13001662

[14] Micro Measurements, Measurement of residual stresses by the hole-drilling strain gage method, Technical Note 11053, Vishay Precision Group (2010).

[15] Scientific Forming Technologies Corporation, DEFORM-2D Version 10.2 User's Manual (August 2011).